TRI-HP PROJECT

Trigeneration systems based on heat pumps with natural refrigerants and multiple renewable sources

Validation of the self-diagnosis efficiency system

Deliverable number: D6.3

Version 1.0

This page is intentionally left blank

Project Acronym:	TRI-HP
Project URL:	http://www.tri-hp.eu
Responsible partner:	IREC
Deliverable nature:	Report (R)
Dissemination level:	Public (PU)
Contractual Delivery Date:	February 28, 2021
Actual Delivery Date	February 28, 2021
Number of pages:	26
Keywords:	Fault detection and diagnosis validation
Authors:	Ivan Bellanco (IREC), Francisco Belío (IREC), Jaume Salom (IREC)
Collaborators:	Thibault Péan (IREC), Raphael Gerber (HEIM/Cadena)
Review:	Daniel Carbonell (SPF-OST)
Approval:	Daniel Carbonell (SPF-OST)

Revision History

Date	Version	Changes
February 28, 2021	v1.0	Version submitted to EC

TRI-HP CONSORTIUM

SPF INSTITUT FÜR SOLARTECHNIK	Oberseestrasse 10 CH-8640 Rapperswil, Switzerland	Coordinator : Dr. Daniel Carbonell Dani.Carbonell@spf.ch
tecnalia Inspiring Business	Área Anardi, 5. E-20730 Azpeitia (Gipuzkoa), Spain	Mr. Andoni Diaz de Mendibil andoni.diazdemendibil@tecnalia. com
...cadena	Murtenstrasse 116, CH-3202, Frauenkappelen, Switzerland	Mr. Raphael Gerber raphael.gerber@cadena.ch
IREC 10 YEARS Shaping Energy for a Sustainable Future	Jardins de les Dones de Negre 1 2ªpl. 08930 Sant Adrià de Besòs (Barcelona)	Dr. Jaume Salom jsalom@irec.cat
ALFA LAVAL	Box 74, 22100 Lund, Sweden	Mr. Mats Nilsson MatsR.Nilsson@alfalaval.com
ILAG swiss quality coatings	Hämmerli 1, CH-8855, Wangen, Switzerland	Mrs. Stephanie Raisch stephanie.raisch@ilag.ch
Institut für sozial-ökologische Forschung	Hamburger Allee 45, Frankfurt am Main, 60486, Germany	Dr. Immanuel Stiess stiess@isoe.de
NTNU Norwegian University of Science and Technology	Kolbjørn Hejes vei 1D (B249), No-034 Trondheim, Norway	Dr. Ángel Álvarez Pardiñas angel.a.pardinas@ntnu.no
DANISH TECHNOLOGICAL INSTITUTE	Kongsvang Allé 29, 8000 Aarhus C, Denmark	Mr. Claus Bischoff claus.bischoff@gmail.com
Hochschule Karlsruhe Technik und Wirtschaft UNIVERSITY OF APPLIED SCIENCES IKKU Institute of Refrigeration, Air-Conditioning and Environmental Engineering	Moltkestr. 30, 76133 Karlsruhe, Germany	Dr. Prof. Michael Kauffeld Michael.Kauffeld@hs-karlsruhe.de
REHVA Federation of European Heating, Ventilation and Air Conditioning Associations	Rue Washington 40, 1050 Brussels, Belgium	Ms. Anita Derjanecz ad@rehva.eu
GR E.F.C. EQUIPOS FRIGORIFICOS COMPACTOS,S.L.	C/Zuaznabar 8 Pol. Ind. Ugaldetxo, Oiartzun, 20180, Spain	Mr. Gabriel Cruz g.cruz@equiposfrigorificoscompactos.com

CONTENTS

EXECUTIVE SUMMARY

This deliverable describes the experimental validation of a fault detection and diagnosis (FDD) method within the TRI-HP project. A self-learning FDD for variable speed heat pump was developed previously and validated with simulated data. In the present work a series of faults were emulated in a real 10 kW variable-speed water-to-water heat pump developed within the project using propane as a refrigerant. The considered emulated faults were: evaporator fouling, liquid-line restriction, compressor valve leakage, refrigerant overcharge and refrigerant undercharge. A comparison between those faults and the no fault situation was made to obtain useful parameters for fault identification. The variables compared, also called features, were the Coefficient of performance (COP), the electrical power consumption, heating power, subcooling, superheating, evaporation and condensation temperatures, discharge line and liquid line refrigerant temperatures, refrigerant mass flow and compressor speed. Those experimental test update the results obtained using simulated data regarding the fault impact on different heat pump variables. In general, every fault decreases the COP and increases the electrical power consumption. The evaporator fouling and liquid line restriction were the faults that have a lower and higher degradation effect on the COP, respectively.

The FDD consist of different modules: the steady-state detector, the input space, the regression model and the diagnosis module. The steady-state detector eliminates non-steady data to increase the prediction efficiency and has worked correctly during the validation. The input space module classifies the data in groups defined by the driving variables. For the validation with simulated data, those driving variables where the compressor speed, the condenser outlet temperature and evaporator inlet temperature. During the experimental tests, the compressor speed changed causing a failure on the algorithm, since it was not able to differentiate if the speed changed due to a fault or due to a change in the heat demand. Therefore, the compressor speed was changed for the condenser inlet water temperature as a driving variable. The regression model represents the heat pump behavior in normal conditions.

The detector was trained with 50 hours of data corresponding to 42 hours of dynamic conditions, 6 and 2 hours of static tests at 10.2 kW and 12.3 kW respectively. For dynamic conditions, a virtual model developed in TRNSYS emulated the demand and the heat source of a residential building in Zurich climate. Once trained, the algorithm predictions were compared with the heat pump measurements. If the residual between both was larger than the training error margin this was an indication of a possible fault. To avoid the false alarms, the possible fault indication must be present 80 % of the time for a 10 minutes period. When a fault is detected a warning flag is triggered. After that, a comparison of the trends of the features is made to diagnose which fault is occurring. The diagnose chart developed previously with simulation data does not work for the current heat pump because of the differences between the simulation and experimental trends. Because of that, the diagnose chart was updated with the obtained experimental trends.

The algorithm detects COP drifts of 7 % in 10 minutes. The detector has high accuracy as shows no false alarms during the tests. The diagnosis module, after the update, could diagnose each fault, except evaporator fouling which was detected as a fault, but without a diagnose.

The FDD run in parallel during those tests giving real-time information about the heat pump soundness. The algorithm run from an industrial computer located in the laboratory. At the same time, it was running in a pocket-size computer called Raspberry Pi [1]. The low computational need of the algorithm allows us to implement it in portable platforms.

List of Acronyms

COP	Coefficient of performance
CVL	compressor valve leakage
DT	Detection time
EF	evaporator fouling
FAR	false alarm rate
FDD	fault detection and diagnosis
FI	fault intensity
FIR	fault impact ratio
HVAC	heating, ventilation and air conditioning
LL	liquid line restriction
lpm	liters per minute
MDR	Missed detection rate
MR	Misdiagnosis rate
OC	refrigerant overcharge
RMSE	root-mean-square error
rps	revolutions per second
SSD	steady state detector
UC	refrigerant undercharge
VSHP	variable speed heat pump

1 INTRODUCTION

The increasing deployment of heat pumps in buildings is expected to contribute to a reduction of energy consumption as the efficiency of these systems is improved compared to alternative heating, ventilation and air conditioning (HVAC) solutions. It is critical to maintain heat pump performance, as fault conditions can affect their optimal operation and reduce their energy efficiency [2]. Field surveys point to significant losses in the performance of heat pumps installed in buildings, with 20 % to 50 % of them operating at 70 % to 80 % efficiency or lower than their design efficiency [3]. Fault operation resulting from anomalous control operation and service deficiencies or components degradation may lead to a lower heat pump performance and increase in power consumption. Within this context, the development of FDD systems for heat pumps is aimed at monitoring, detecting and identifying operation faults. The development of such fault monitoring systems requires the availability of experimental and simulated data for training and validating FDD methods under fault-free and faulty conditions.

Comparison among different works has shown significant similarity regarding system behaviour for fixed speed compressor heat pumps under fault conditions. However, only a few studies have focused on analysing the influence of faults on variable speed heat pump performance. These few studies indicate that the behaviour of these systems substantially differs from that of fixed speed heat pumps, due to the regulation of the compressor operation, which leads to a different degree of fault impact on the operation variables. Requirements by international regulations to increase efficiency are leading to a replacement of fixed-speed heat pumps by more efficient inverter-driven heat pumps in the residential market. Thus, it is necessary to conduct more research to investigate the influence of faulty operation on the performance of variable speed systems and derive methods for the development of FDD methodologies specific to these systems.

One challenge in assessing the impact of faults on variable speed heat pumps is the lack of literature publications on the influence of faulty operation on the operating variables of this type of equipment. In order to solve this issue, in this work, an experimental campaign with a variable speed heat pump was made. A 10 kW variable speed propane heat pump was tested with no fault present and with emulated faults. The impact of each fault was determined. In this way, the FDD developed has been validated with real data. The fault test took into account static and dynamic conditions. For the dynamic tests, a virtual model provided dynamic demand to test the FDD under more realistic conditions.

This deliverable is structured in 4 sections. The first one describes the test facility and the experimental procedure for emulating each fault. The second compares the fault impact in different heat pump features. The third section shows the results and the validation of the different parts involved in the FDD. The last section exposes the conclusions and the future steps for the FDD.

2 METHODOLOGY

This section explains the details of the experimental campaigns for testing the performance of the FDD. First a description of the test facility and test rig is provided. Next, the static tests made for rating the performance of the heat pump are summarized. Finally, the faults tested and the emulation procedure are explained.

2.1 THE SEMI-VIRTUAL ENERGY INTEGRATION LABORATORY - SEILAB

2.1.1 General introduction

The SEILAB [4] provides advanced methods to assess the development and integration of renewable energy solutions and innovative thermal and electrical equipment that are designed to improve energy efficiency in buildings and energy systems.

It is equipped with cutting-edge technology comprising systems for energy generation, heat and cold storage and state-of-the-art facilities for testing HVAC equipment and the interaction of energy systems with the grid.

The operation is based on a semi-virtual testing approach, which allows for real equipment to be operated as a function of the behaviour of a dynamic virtual model (hardware-in-the-loop concept) that emulates the thermal loads of heat sink and heat source.

The SEILAB is pioneer in addressing the smart integration of electrical and thermal components and is a leading experimental facility for improving the development of Net Zero Energy Buildings and Energy Flexible buildings.

2.1.2 Description of test facilities

2.1.2.1 Test benches and primary heat exchangers

Each hydraulic loop comprises one test bench and one or more primary heat exchangers. The function of test benches is to measure pressure and temperature, and to measure and control flow. One of the temperature measurements is used for loop temperature control in the primary heat exchanger unit. Primary heat exchanger units include as well the heat exchanger itself and a circulating pump driven by a frequency inverter.

Flow and temperature meters are regularly calibrated to allow an accurate calculation of thermal power. Table 2.1 indicates type and precision of the different measurement elements.

Table 2.1: SEILAB measurements precision

Magnitude	Type	Precision
Pressure	Piezo-resistive	±1%
Flow	Electromagnetic	±0.5%
Temperature	3- or 4-wire Pt100	±0.25 K
Electrical power	Multimeter	±1%

Three-way mixing valves with fast magnetic actuator are used to control flow and temperature. One of the inlets is a by-pass of the tested equipment (flow) or the heat exchanger (temperature).

Heat transfer fluid is soft water free of suspended solid particles. Pipes are insulated with synthetic rubber material (30 mm).

2.1.2.2 Data acquisition and control

The tests performed in SEILAB are supervised and controlled by a data acquisition and control system created with the software LabVIEW (Figure 2.1). A custom interface is made for each project, adapting it to the necessities. This interface can be connected to transient simulation software TRNSYS to simulate dynamic conditions. The propane heat pump with a desuperheater is connected with this interface through a Modbus TCP/IP connection for control and monitoring purposes. The FDD algorithm was coded in Python and ran in an industrial computer exchanging data with the laboratory interface. In parallel, a Raspberry Pi [1] worked with the same algorithm. The results are the same for both implementations, showing that the algorithm requires low computational resources.
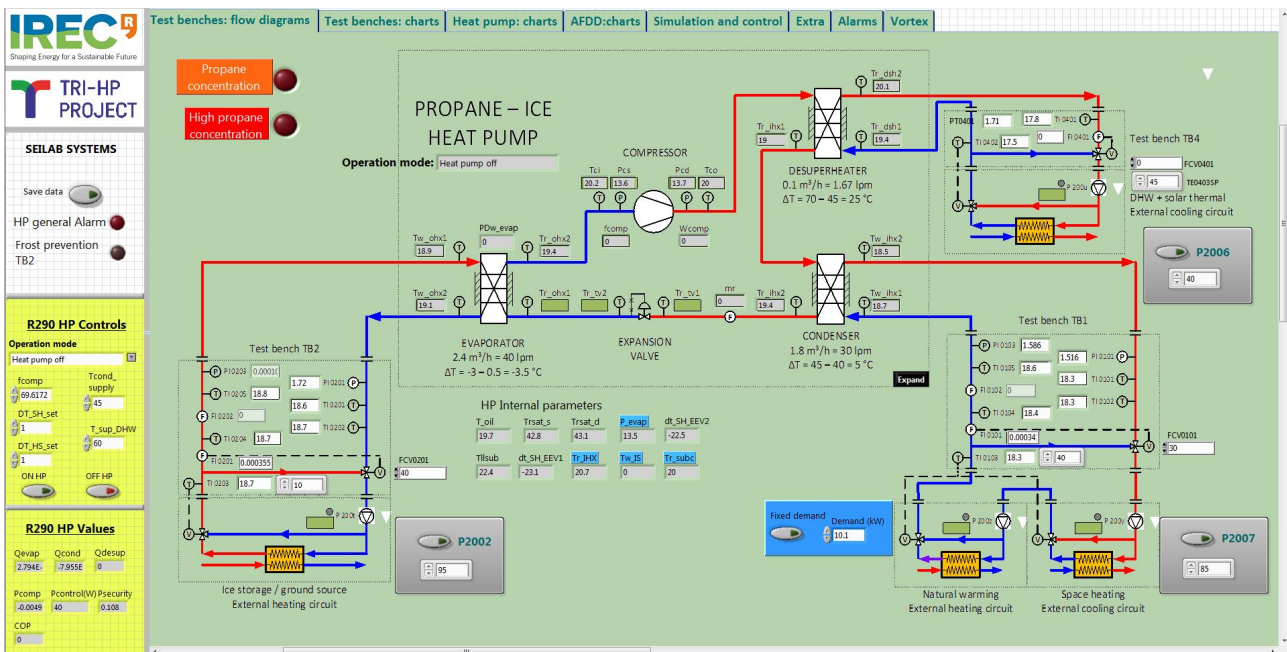
Figure 2.1: TRI-HP project laboratory interface

2.1.2.3 Propane safety system

Due to the flammability of the selected refrigerant R-290 (propane), there is a safety system in the SEILAB to prevent the formation of flammable/explosive atmospheres. It includes automatic gas detection and automatic or manual extraction to a safe area along with measures to remove ignition sources and to limit hazardous consequences.

2.2 TESTING METHOD

2.2.1 Performance rating tests

SPF first tested the propane heat pump under conditions defined in the European standards EN 14511:2018, EN 14825:2016 and EN 16147:2017. Some of these tests are replicated in SEILAB to ensure that the refrigeration charge or other boundary conditions of the heat pump have not affected the performance. The heat pump was designed

to work with near-zero temperatures in the evaporator (average evaporator temperature in the range 2 °C to 8 °C). Therefore, this circuit must be filled with brine. However, the experimental campaign in SEILAB was designed to work with average evaporator temperatures in the range of 6 °C to 14 °C. Because of that, the evaporator circuit was filled with just water at SEILAB. Taking this into account, static tests at SEILAB have different conditions that the ones in SPF.

The standard EN 14511:2018 for space heating test asks for a temperature of 0 °C in the evaporator inlet for brine heat pumps. For water heat pumps, this temperature is 10 °C. Those two temperatures are the "rating conditions" of the standard. This means fixed supply and return temperatures in evaporator and condenser while the flows are the ones that maintain a specific temperature difference in the evaporator and condenser. Then, the standard defines the "application conditions" where the supply temperatures are fixed, the flows are those obtained in the rating conditions and the return temperatures are not controlled. The frequency of the compressor was set to 70 revolutions per second (rps), corresponding to 10 kW of heating capacity. Figure 2.2 shows a comparison between IREC and SPF results. As can be seen, the results of both facilities are similar and follow the same trend.
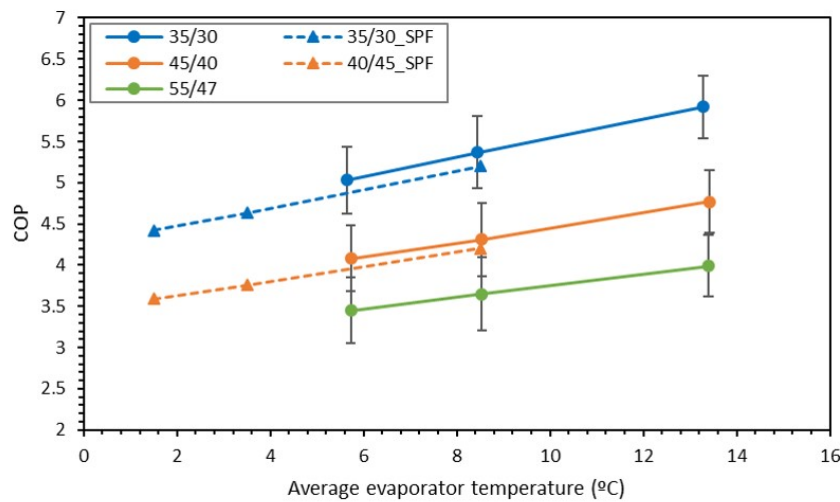
Figure 2.2: Space heating rating tests for compressor speed of 70 rps. The series name represent the supply and return temperatures of the condenser.

2.2.2 Fault tests

The FDD is validated with the emulation of common faults in heat pumps. The selected faults for the validation are refrigerant undercharge (UC), refrigerant overcharge (OC), compressor valve leakage (CVL), liquid line restriction (LL) and evaporator fouling (EF).

The heat pump has been provided without compressor speed control. However, it was implemented the possibility to send a frequency set point to the compressor. The FDD designed is specific for variable speed heat pump (VSHP). Because of that, a PID control has been developed using the condenser outlet water temperature to adapt the speed of the compressor in order to reach the supply temperature set-point. All the faults were emulated in three different conditions: two static tests and one dynamic test.

For the static tests, return temperature in the condenser was set to 40 °C and 39 °C, corresponding to demands of 10.2 kW and 12.3 kW, respectively. The supply temperature of the heat pump was set to 45 °C, the evaporator return temperature to 10 °C. The water flows of the evaporator and condenser were set to 40 lpm and 30 lpm, respectively. Table 2.2 shows those conditions.

Table 2.2: Static tests conditions. From the water side: condenser outlet temperature ($T_{cond,out}$), condenser inlet temperature ($T_{cond,in}$), evaporator inlet temperature ($T_{evap,in}$), condenser water flow ($\dot{V}_{cond}$) and evaporator water flow ($\dot{V}_{evap}$).

Heating Load (kW)	$T_{cond,out}$ (ºC)	$T_{cond,in}$ (ºC)	$T_{evap,in}$ (ºC)	$\dot{V}_{cond}$ (lpm)	$\dot{V}_{evap}$ (lpm)
10.2	45	40	10	30	40
12.3	45	39	10	30	40

The dynamic test uses a virtual model of a 100 m^2 fully insulated single-storey detached house with boreholes. The climate selected is Zurich. Figure 2.3 shows the expected temperatures of the circuits and the thermal loads. The model read the supply temperatures and the water flows in the evaporator and condenser and send the return temperatures for both.
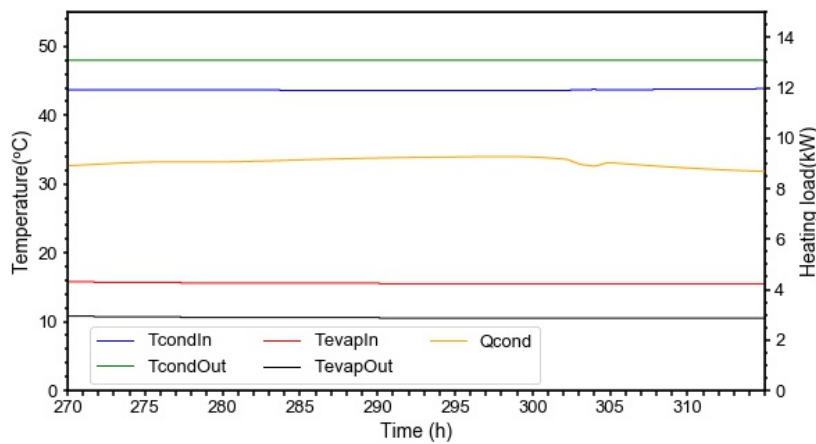
Figure 2.3: Graph with the demand (Q_{cond}), inlet and outlet evaporator temperatures ($T_{evap,in}$, $T_{evap,out}$) and inlet and outlet condenser temperatures ($T_{cond,in}$, $T_{cond,out}$) for the TRNSYS model with the Zurich climate from the water side.

The desuperheater and the subcooler were not used in the static and dynamic tests. Each fault was tested in both dynamic and static conditions. An additional no-fault test is made in every set-up to serve as a reference.

2.2.2.1 Evaporator fouling

The evaporator fouling represents a circulating pump malfunction or the accumulation of dirt in the circuit that reduces the evaporator flow. This fault is emulated reducing the water flow of the evaporator below the nominal. The indicator fault intensity (FI) is used to characterize each fault stage. The FI_{EF} is shown in Equation 2.1.

$$FI_{EF} = \frac{\dot{V}_{fault} - \dot{V}_{nom}}{\dot{V}_{nom}} \qquad (2.1)$$

where $\dot{V}_{fault}$ is the evaporator water flow for the current fault level and $\dot{V}_{nom}$ is the water flow for the no-fault condition. Taking into account that the $\dot{V}_{nom}$ is 40 lpm, the Table 2.3 shows the experimental plan followed for the static tests.

Table 2.3: EF static tests experimental plan. The duration of each test is one hour.

Code	Load (kW)	FI	Evaporator water flow (lpm)
EF10.1	10.2	-0.100	36.0
EF10.2	10.2	-0.157	33.7
EF10.3	10.2	-0.214	31.4
EF10.4	10.2	-0.271	29.2
EF10.5	10.2	-0.328	26.9
EF10.6	10.2	-0.385	24.6
EF10.7	10.2	-0.442	22.3
EF10.8	10.2	-0.500	20.0
EF12.1	12.3	-0.100	36.0
EF12.2	12.3	-0.157	33.7
EF12.3	12.3	-0.214	31.4
EF12.4	12.3	-0.271	29.2
EF12.5	12.3	-0.328	26.9
EF12.6	12.3	-0.385	24.7
EF12.7	12.3	-0.442	22.3
EF12.8	12.3	-0.500	20.0

2.2.2.2 Compressor valve leakage

The compressor valve leakage fault represents the bypass of refrigerant between the high and low-pressure sides. This leakage can appear in the compressor or in the reversing valves. A pipe that bypasses the suction and discharge lines of the compressor was installed to emulate the fault. A valve allows to open or close the line. Figure 2.4 shows a schematic of the bypass and a picture of the valve with an indicator of the turned angle.

The FI for this fault is shown in Equation 2.2.

$$FI_{CVL} = \frac{\dot{m}r_{fault} - \dot{m}r_{nom}}{\dot{m}r_{nom}} \tag{2.2}$$

Where $\dot{m}r_{fault}$ is the refrigerant mass flow for the fault condition and $\dot{m}r_{nom}$ is the refrigerant mass flow when no fault is present. As the heat pump has a variable-speed compressor, $\dot{m}r_{nom}$ depends on the speed of the compressor. A correlation between compressor speed and refrigerant mass flow was obtained by running the compressor at different speeds without fault present. The test was made for both capacities, obtaining Equation 2.3. This equation relates the compressor frequency in rps and the refrigerant mass flow in g/s for no-fault conditions. This equation is used to give an approximate value of the FI. It may lose precision with faults present or different capacities.

$$mr_{nom} = 0.5206 \cdot freq + 0.7082 \tag{2.3}$$
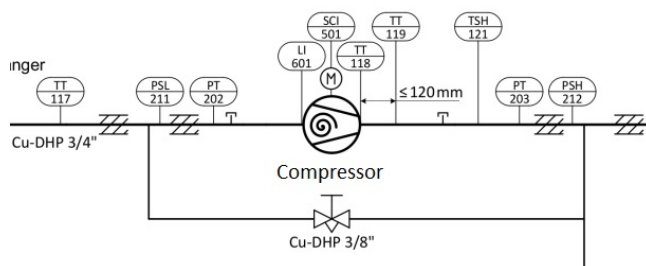
Figure 2.4: Scheme and picture of the bypass between suction and discharge lines of the compressor. An indicator was made to serve as a goniometer.

The experimental plan is shown in Table 2.4. During the experimental campaign, the correlation between frequency and refrigerant mass flow was not known. Because of this, each fault step was reproduced by turning the valve a certain amount of degrees without knowing the FI exactly. The valve count with a maximum stroke of 90°, meaning that there is a low margin for each fault step. Because of that, different fault levels have the same FI. The FI column was obtained from Equatoin 2.3 .

Table 2.4: CVL static tests experimental plan. The duration of each test is one hour.

Code	Load (kW)	Valve stroke (°)	FI
CVL10.1	10.2	9.0	0.00
CVL10.2	10.2	13.5	0.00
CVL10.3	10.2	18.0	0.00
CVL10.4	10.2	22.5	-0.04
CVL10.5	10.2	27.0	-0.29
CVL10.6	10.2	31.5	-0.37
CVL10.7	10.2	36.0	-0.65
CVL12.1	12.3	13.5	-0.02
CVL12.2	12.3	18.0	-0.02
CVL12.3	12.3	22.5	-0.02
CVL12.4	12.3	27.0	-0.13
CVL12.5	12.3	31.5	-0.38
CVL12.6	12.3	34.0	-0.61

2.2.2.3 Liquid line restriction

The liquid line restriction appears when the filter located in the liquid line is clogged. To emulate this fault, the manufacturer placed a restriction valve in the liquid line to increase the pressure drop. Figure 2.5 shows a picture of the restriction valve with an indicator to know the turned degrees.
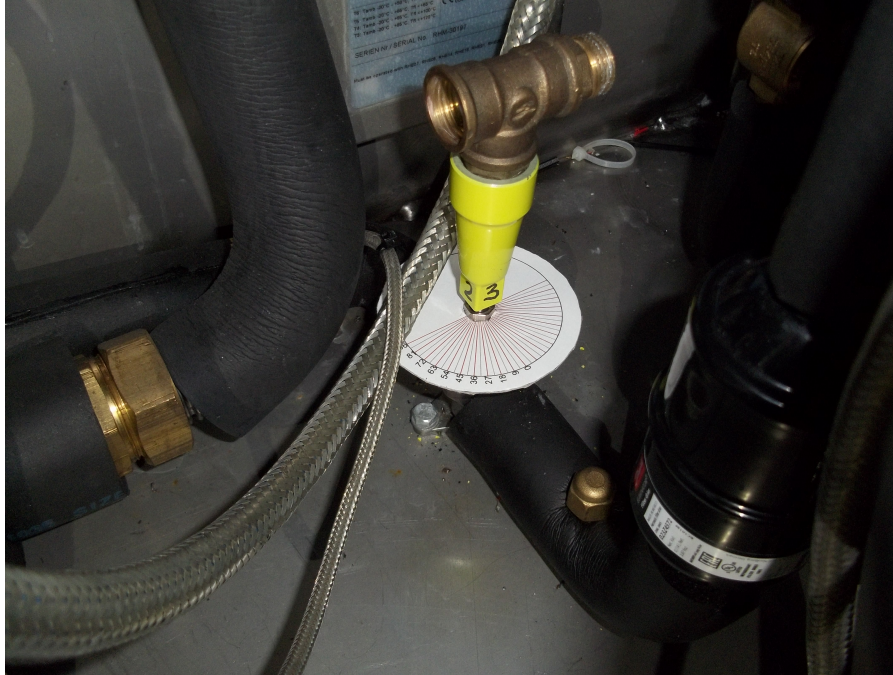
Figure 2.5: Picture of the restriction valve in the liquid line with an indicator to serve as a goniometer.

The FI of this fault is related to the pressure drop variation of the liquid line as Equation 2.4 shows.

$$FI_{LL} = \frac{\Delta P_{LL}}{\Delta P_{nom}} \tag{2.4}$$

Where ΔP_{LL} represents the liquid line pressure drop with fault and ΔP_{nom} the liquid line pressure drop without fault.

The experimental plan is showed in Table 2.5. The fault emulation procedure is the same as the CVL fault, turning the corresponding valve. The planning takes into account the number of turned degrees of the valve but not the FI. This valve has a maximum stroke of three turns and three-quarters. There was not any change in the heat pump until three and a half turns was made. Therefore, the degrees showed in the table start from this position.

2.2.2.4 Refrigerant over-and-under-charge

The refrigerant overcharge fault may appear during a maintenance service because the heat pump is filled with more refrigerant than recommended by the manufacturer. To emulate it, the heat pump was overcharged 10% over the nominal amount. The refrigerant undercharge may appear due to a refrigerant leakage or a maintenance service that reduces the refrigerant charge below the manufacturer's recommendation. To emulate it, the heat pump was undercharged a 10% and a 20% of the nominal amount. The FI is the relative difference between the current and the nominal charge, as Equation 2.5 shows.

$$FI_{OC,UC} = \frac{mr_{fault} - mr_{nom}}{mr_{nom}} \tag{2.5}$$

Table 2.5: LL static tests experimental plan. The duration of each test is one hour, except LL12.5 that is half hour. The valve stroke column takes into account that the initial valve position is at three and a half turns.

Code	Load (kW)	Valve stroke (°)
LL10.1	10.2	45.0
LL10.2	10.2	54.0
LL10.3	10.2	58.5
LL10.4	10.2	63.0
LL10.5	10.2	67.5
LL10.6	10.2	72.0
LL12.1	12.3	54.0
LL12.2	12.3	58.5
LL12.3	12.3	63.0
LL12.4	12.3	67.5
LL12.5	12.3	72.0

Where mr_{fault} is the propane charge for faulty conditions, and mr_{nom} is the nominal propane charge. Table 2.6 shows the experimental plan.

Table 2.6: OC and UC static tests experimental plan. The duration of each test is one hour.

Code	Load (kW)	FI
OC10.1	10.2	0.1
OC12.1	12.3	0.1
UC10.1	10.2	-0.1
UC10.2	10.2	-0.2
UC12.1	12.3	-0.1
UC12.2	12.3	-0.2

3 FAULT IMPACT ON HEAT PUMP PERFORMANCE

From the different measurements of a heat pump, the ones more useful for the FDD are called features. The features selected for the present work are the COP, W_{comp}, Q_{heat}, T_{sc}, T_{sh}, T_{evap}, T_{cond}, T_{ll}, T_{co}, mr and f. Table 3.1 shows the nomenclature of the different measurements.

Table 3.1: Features from the heat pump.

Measurement	Description
W_{comp}	Compressor electrical power consumption
f	Compressor frequency
T_{co}	Compressor discharge temperature
T_{ll}	Liquid-line temperature
mr	Refrigerant mass flow rate
COP	Coefficient of performance
Q_{heat}	Thermal power
T_{sc}	Subcooling
T_{sh}	Superheating
T_{evap}	Evaporation temperature
T_{cond}	Condensation temperature

For the development of the diagnosis module of the FDD, a review of heat pump fault testing and simulation on VSHP was made [5, 6, 7]. To extend the knowledge on the performance of inverter-driven units under faulty conditions, simulations were performed for a variable-speed, water-to-water, propane heat pump. The heat pump modelled was developed using Modelica object-oriented programming language in Dymola simulation environment (Dassault Systems, Vélizy-Villacoublay, France). From the literature and simulation analysis, the expected trends of a heat pump are showed in Table 3.4 in the grey shadowed rows. This results were applied to a TRNSYS simulation model of an air-to-water, variable speed heat pump with R407. A parametrization method was used to obtain faulty data from the TRNSYS model. The diagnosis module was validated with the simulation results.

Tables 3.2 and 3.3 shows the average values of each feature for the 10.2 kW and 12.3 kW static tests, respectively. In some tests as in CVL10.1, the COP values are higher than in the no fault case because of slight changes in the test condition as a warmer desuper-heater.

Table 3.2: Average values for different features of the heat pump during the 10.2 kW static tests.

Units	COP	W_{comp} (kW)	Q_{heat} (kW)	T_{sc} (K)	T_{sh} (K)	T_{evap} (°C)	T_{cond} (°C)	T_{co} (°C)	T_{ll} (°C)	mr (g/s)	f (rps)
NF10	4.40	2.20	10.20	2.0	11.0	4.5	46.8	63.4	44.6	29.60	57
EF10.1	4.41	2.10	10.15	2.0	11.0	4.5	46.5	63.3	44.4	29.48	57
EF10.2	4.40	2.10	10.16	1.9	11.0	4.3	46.5	63.4	44.5	29.47	57
EF10.3	4.37	2.10	10.16	1.9	11.0	4.0	46.5	63.5	44.6	29.51	57
EF10.4	4.34	2.10	10.17	2.0	11.0	3.8	46.5	63.6	44.4	29.58	58
EF10.5	4.30	2.10	10.16	1.8	11.0	3.4	46.5	63.7	44.6	29.49	58
EF10.6	4.26	2.20	10.15	1.9	11.0	3.2	46.5	63.9	44.5	29.47	59
EF10.7	4.22	2.20	10.15	2.2	11.0	2.7	46.5	64.1	44.3	29.67	59
EF10.8	4.16	2.20	10.16	2.2	11.0	2.2	46.5	64.3	44.2	29.65	60
CVL10.1	4.46	2.14	10.16	2.1	11.0	4.8	46.8	63.2	44.6	29.39	56
CVL10.2	4.46	2.14	10.16	1.8	11.0	4.8	46.5	63.2	44.6	29.44	56
CVL10.3	4.46	2.14	10.16	1.7	11.0	4.8	46.5	63.2	44.6	29.41	56
CVL10.4	4.31	2.21	10.14	2.2	10.7	5.0	46.5	64.1	44.2	29.30	58
CVL10.5	3.43	2.82	10.14	6.7	9.8	5.4	46.8	74.2	40.2	27.36	72
CVL10.6	3.12	3.12	10.16	7.0	9.9	5.5	47.0	80.2	40.1	26.50	78
CVL10.7	3.50	2.78	5.93	4.2	9.7	9.9	44.3	100.5	40.1	13.86	73
LL10.1	4.54	2.10	10.15	4.0	10.7	4.8	46.7	63.2	42.8	29.35	55
LL10.2	4.10	2.33	10.15	8.4	11.0	0.9	48.3	68.4	40.0	27.97	60
LL10.3	3.80	2.53	10.15	9.6	12.7	-1.8	49.5	72.8	40.0	27.32	63
LL10.4	3.61	2.68	10.15	11.3	14.3	-3.3	51.2	76.9	40.1	26.74	66
LL10.5	3.27	2.96	10.15	14.4	17.0	-6.0	54.3	84.9	40.1	25.83	70
LL10.6	2.87	3.40	10.15	21.7	20.0	-8.8	61.7	98.2	40.1	24.28	73
OC10	3.49	2.63	10.12	24.9	10.7	7.0	64.8	84.8	40.0	28.65	51

The quantitative results are synthesized in Table 3.4, which shows different features trends for each fault obtained during the experimental campaign. From the experimental campaign, we have determined that the compressor frequency must be a key feature to take into account as it is one of the most affected parameters by the faults. However, in the literature analysis it was not taken into account. As can be seen, there are some discrepancies between the literature and the experiments. In some cases, features that in the literature shows no change, are affected in the tests. Those discrepancies are because of the scarce literature about experimental fault tests with variable heat pumps. The only contradictory result is the T_{sc}, in LL is decreasing in the literature but increasing in the tests. This trend is adapted from [8], from a fixed capacity, short tube orifice rooftop air conditioner. Different heat pump technologies as water-to-water and air-to-air, or cooling and heating mode have different fault repercussions. Therefore, the present work is valid for water-to-water, heating mode heat pumps, but could not work with transcritical cycles or other heat pump typologies. Below, there is an explanation of how each fault has affected the heat pump in the experimental campaign.

Table 3.3: Average values for different features of the heat pump during the 12.3 kW static tests.

Units	COP	W_{comp} (kW)	Q_{heat} (kW)	T_{sc} (K)	T_{sh} (K)	T_{evap} (°C)	T_{cond} (°C)	T_{co} (°C)	T_{ll} (°C)	mr (g/s)	f (rps)
NF12	4.39	2.60	12.30	4.1	8.7	4.1	46.9	61.9	42.6	35.90	69
EF12.1	4.36	2.60	12.26	4.0	8.7	3.8	46.9	62.0	42.7	35.69	69
EF12.2	4.34	2.60	12.26	4.0	8.7	3.6	46.9	62.0	42.7	35.76	69
EF12.3	4.31	2.60	12.26	4.1	8.7	3.4	47.0	62.0	42.7	35.69	70
EF12.4	4.28	2.64	12.27	4.1	8.8	3.1	46.9	62.2	42.6	35.71	70
EF12.5	4.24	2.68	12.27	4.1	8.9	2.7	46.9	62.4	42.5	35.90	71
EF12.6	4.20	2.70	12.27	4.2	9.4	2.3	46.8	62.8	42.4	35.89	72
EF12.7	4.14	2.70	12.26	4.3	9.9	1.8	46.8	63.3	42.4	36.00	72
EF12.8	4.08	2.80	12.26	4.5	10.2	1.2	46.8	63.7	42.3	36.14	73
CVL12.1	4.39	2.59	12.25	4.1	8.6	4.1	47.0	61.9	42.7	35.75	69
CVL12.2	4.39	2.59	12.26	4.0	8.6	4.1	46.9	61.8	42.8	35.76	69
CVL12.3	4.38	2.58	12.25	4.7	8.5	4.2	47.0	62.1	42.2	35.65	69
CVL12.4	3.90	2.90	12.24	6.5	8.7	4.5	47.0	66.3	40.5	35.10	76
CVL12.5	3.04	3.60	11.73	8.3	9.5	4.8	47.3	82.5	39.2	30.08	92
CVL12.6	2.31	3.36	8.27	7.2	10.6	5.0	46.2	105.0	39.2	18.47	89
LL12.1	4.28	2.72	12.24	8.8	11.1	2.2	47.8	66.6	39.1	34.26	69
LL12.2	3.83	3.07	12.28	10.7	11.9	-1.3	49.7	71.5	39.1	33.67	75
LL12.3	3.57	3.30	12.28	13.2	13.9	-3.3	52.2	77.0	39.1	32.79	78
LL12.4	3.35	3.52	12.26	15.8	15.4	-4.7	54.8	82.5	39.1	31.93	81
LL12.5	3.02	3.93	12.30	21.2	17.8	-7.0	60.2	92.3	39.1	30.60	84
OC12	3.57	3.28	12.22	25.7	9.9	6.8	64.6	83.5	39.1	34.76	62

Table 3.4: Trends of different features of the heat pump. Minus symbols are applied for decreasing trends. Plus symbols are applied for increasing trends. The results coming from the literature research (lit.) are grey shadowed.

	COP	W_{comp}	Q_{heat}	T_{sc}	T_{sh}	T_{evap}	T_{cond}	T_{co}	T_{ll}	mr	f
OC test	-	+	=	+ +	=	+ +	+ +	+ +	-	=	-
OC lit.	-	+	=	+			+			-	
CVL test	-	+ +	-	+	=	=	=	+ +	-	-	+ +
CVL lit.	-	+	=	=	+			+		-	
EF test	-	+	=	=	=	-	=	=	=	=	+
EF lit.	-	+	=			-		+			
LL test	- -	+ +	=	+ +	+ +	- -	+ +	+ +	-	-	+
LL lit.	-	+	=	-	+				+		
Criteria											
+ +, - -	±1	±0.5 kW	±1 kW	±5 °C	±5 °C	±5 °C	±5 °C	±5 °C	±5 °C	±5 g/s	±15 rps
+ , -	±0.1	±0.1 kW	±0.2 kW	±2 °C	±2 °C	±2 °C	±2 °C	±2 °C	±2 °C	±2 g/s	±3 rps
+,-				±1 °C	±1 °C	±1 °C	±1 °C	±1 °C	±2.5 °C	±50 g/s	

The OC fault increases the liquid trapped in the condenser, raising the condensation temperature. The evaporation temperature increases due to a 0.4 bars increase of the suction pressure. The subcooling and the compressor

outlet temperatures increases. The refrigerant mass increase, reduces the speed of the compressor maintaining the same mass flow in the circuit.

The CVL fault increases the pressure at the suction line while the discharge pressure remains the same. To compensate all the refrigerant that goes through the bypass, the compressor increases the speed, increasing the power consumption and the compressor outlet temperature. The superheating is maintained by the expansion valve but it increases for higher demands. For higher fault values, the refrigerant mass in the circuit is very low and the demand can not be covered.

The EF reduces the evaporator pressure while the evaporator outlet temperature increases, remaining the sub-cooling the same and decreasing the evaporation temperature. The compressor speed increases to cover the demand.

The LL causes an additional pressure loss between condensation pressure and suction pressure. This can lead to limited capacity of the expansion valve with the consequence of lower suction pressure and higher condensation pressure. This increases the condensation temperature,the superheating and the subcooling while decreases evaporation temperature. As the literature [7] results are for an air-to-air heat pump this could explain the discrepancies.

The UC fault was tested according to the experimental plan of section 2.2.2. A charge reduction of 10 and 20 % was made, but the pressure of the circuit remained very high. This could be an indicator of an additional fault as non-condensables present in the circuit due to the consecutive charge procedures or another underlying fault. Because of this, the results are not presented.

All the faults decreased the COP of the heat pump, being EF the fault that had less effect and LL the one that had the highest. As the heating power is usually not affected, the decrease in COP comes from an increase in electric power consumption. The heating power could be maintained for all the faults except in the higher fault levels of CVL.

4 Results on the validation of the FDD system

4.1 Introduction

In this chapter, the validation of a FDD algorithm with the data obtained from the experimental fault emulation is shown. This algorithm has been previously developed and validated with simulation data. The algorithm consists of different modules whose operation are described below.

The algorithm starts with the training phase in which the FDD learns the heat pump operation at fault free conditions. During the learning period of one week, the data measured will be filtered by the steady-state detector, so that only the stationary points will be stored. After the training period, the stored data will be classified using pre-defined ranges for the independent features of the input space module as condenser outlet and inlet temperature and evaporator inlet temperature, which are the input variables to the regression models. A regression model will be trained for each of these regions of the input space. During the training, the root-mean-square error (RMSE) is obtained for each of the models and this value is used to define the error of the prediction.

Once the system has learnt normal operation for the specific heat pump, the monitoring phase starts. As in the learning period, during this phase, measurements from the different sensors are filtered by the steady-state detector and the steady-state data is classified according to the input space structure. If the data has no associated regression model, i.e., the data is beyond the limits of the data obtained during the training period, it will be stored until enough data points (equivalent to one hour of data) are stored for training the new region, re-activating self-training. If the data belongs to the data range from the learning phase, the corresponding regression model will predict the features for the given input conditions at each time step. The features measured with the different sensors and those predicted by the FDD regression model are compared, obtaining the residuals. If the residuals are above or below of the error margin, it is considered that the current measurements deviate from the no-fault behaviour. However, outliers, fluctuations or measurement errors can deviate from the prediction, thus, for triggering a warning flag several deviations from ideal performance must be accumulated during a certain time. Only when the fault ratio (rate of total number of events considered faulty over a sample) is above 80% a warning flag is triggered. In the event of a warning, the residual of each of the features with respect to the model prediction is used for fault identification using a trend chart method. The trend comparison of the different features is used to diagnose the cause of the fault. Figure 4.1 shows a simplified scheme of the algorithm structure. With the real time data, the steady state detector, input space, regression model, fault monitoring and fault diagnosis are validated running the algorithm in a computer and also in a Raspberry pi. As the test are isolated between them, the retraining is deactivated for the present work. For the same reason, the training data is fed to the algorithm in a file rather than in a real-time learning period.
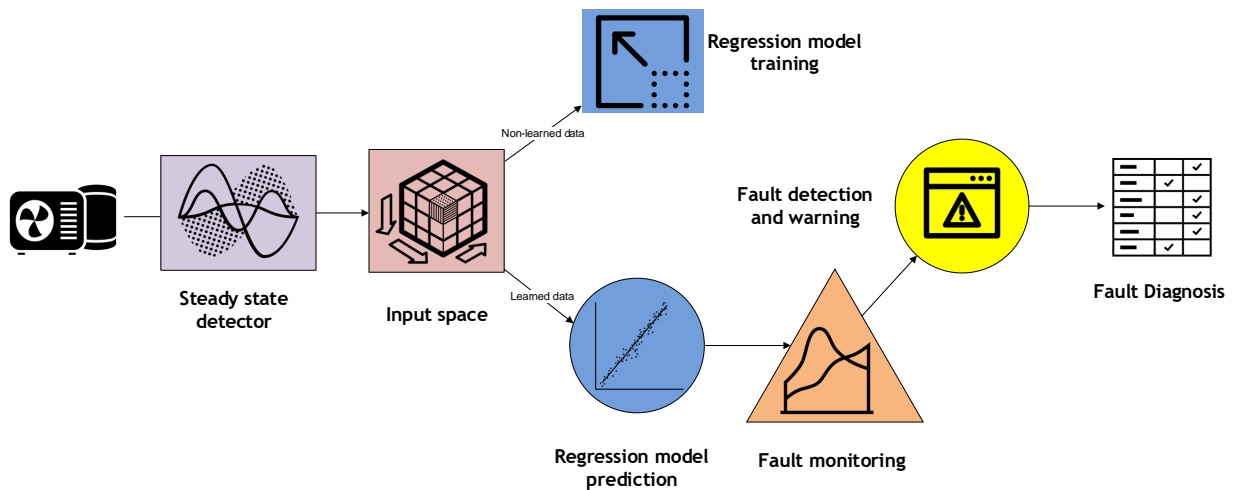
Figure 4.1: General scheme of the FDD algorithm.

4.2 STEADY STATE DETECTOR

The steady state detector eliminates the non-stationary data of the measurements to improve the results of the regression method. The steady state detector (SSD) developed works with the mean and the variance of a data series analyzing its trend in different data-windows.

Figure 4.2a shows the steady-state detection in the condenser load signal. The detection is relatively constant with interruptions due to the detection criteria. Figure 4.2b shows the detection on a series with noise. As can be seen, the outlier is filtered by the detector. The detector is designed to prioritize noise filtering. However, it could discard possible steady data.
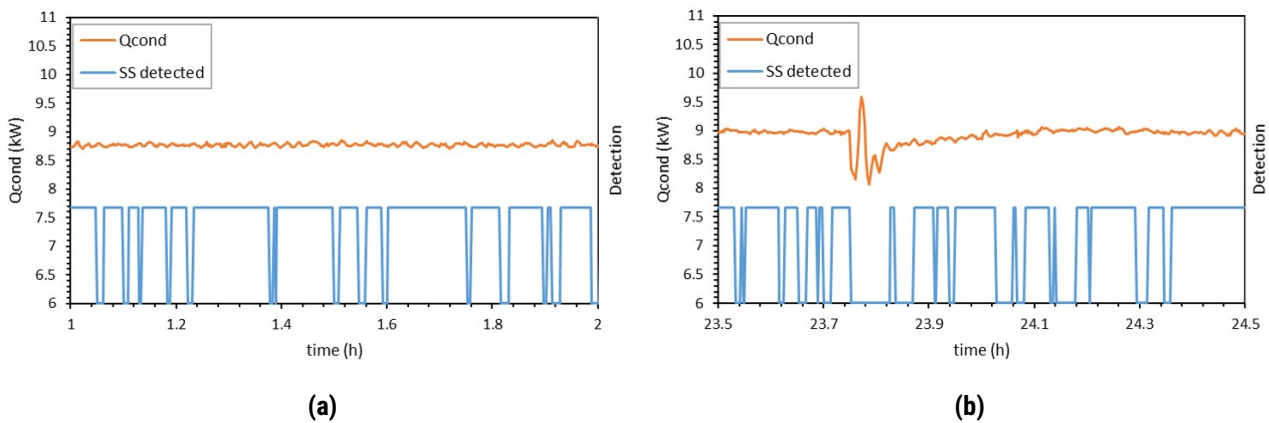

Figure 4.2: Detection of steady-state points in the condenser load signal. a) steady signal, b) signal with outliers.

4.3 Input space

The input space classifies the data to improve the accuracy of the regression model. The data is classified in a three-dimensional space defined by the driving variables of the heat pump. For an air-to-water heat pump, those variables are: the condenser outlet temperature, ambient temperature and the compressor speed. The driving variables are external to the heat pump operation. For a water-to-water heat pump, we selected the condenser outlet and evaporator inlet temperatures and compressor speed. After some experiments, we realized that compressor speed is an internal control of the heat pump. The heat pump will adapt the compressor speed, trying to achieve the load requirements in the event of a fault. Therefore, if the compressor speed changes, the algorithm can't tell if it's because of a load change or because of a fault. Therefore, instead of compressor speed we use the condenser inlet temperature. Figure 4.3 shows the classification of the training data.
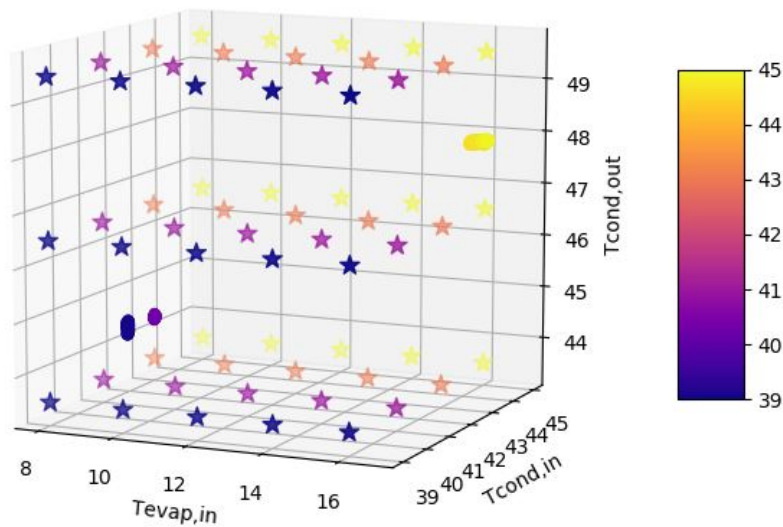

Figure 4.3: Three-dimensional space generated by the Input space module. The stars are the center of each group. The points are the training data. The color scale is used in the $T_{cond,in}$ axis.

4.4 Regression method and fault detection

4.4.1 Regression model training

The regression model was trained with heat pump data with no fault present. To obtain predictions for different conditions, the model was trained with the two static conditions (10.2 kW and 12.3 kW) and the dynamic model. The dynamic test was two consecutive days with the TRNSYS simulation model explained in Section 2.2.2. However, the test was interrupted by an equipment disconnection and was retaken starting the simulation from the last point. Figure 4.4 shows the COP values for the training series. The three different series were put together in a single dataset and fed to the algorithm for training.
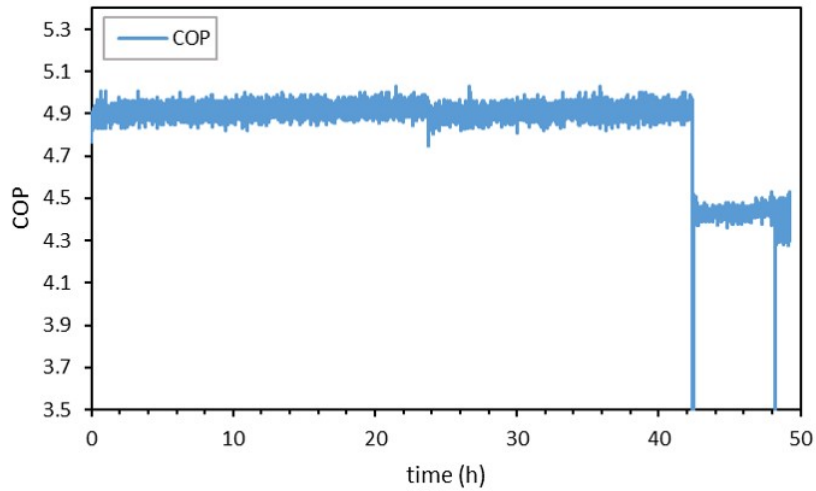
Figure 4.4: COP data used for training the regression model. The signal from 0 h to 42 h correspond to the dynamic test, from 42 h to 48 h the 10.2 kW static test and the rest to 12.3 kW static test. The signal goes to 0 to mark each situation.

For the training data, three different clusters were trained, corresponding to each of the test conditions. Table 4.1 shows each of these clusters and the error margin of the predictions. This margin is obtained as two times the maximum RMSE of the cluster training. This RMSE is the error between the training prediction and the training values. For these clusters, the error margin is below 0.26 units that represents a 5% drift for a 4.5 COP. Figure 4.5 shows the training predictions for the cluster 1. The orange-shadowed area corresponds to the error margin of the prediction.

Table 4.1: Clusters obtained from the algorithm training.

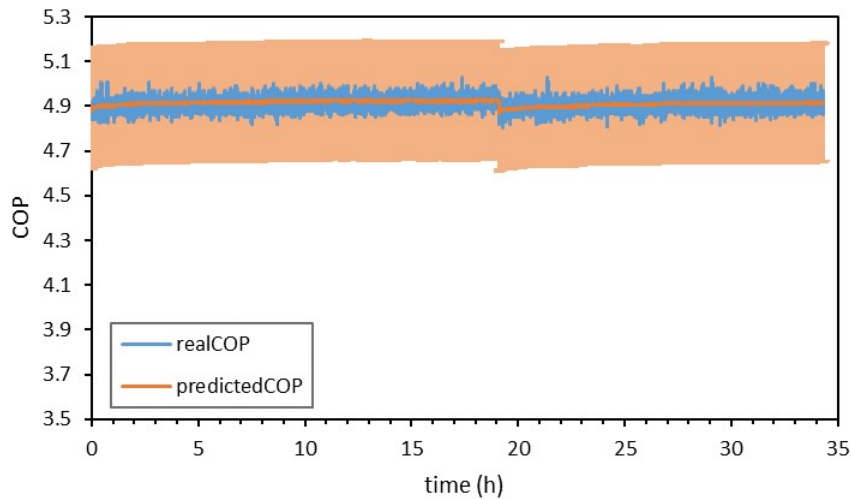| Cluster	$T_{evap,in}$ (ºC)	$T_{cond,in}$ (ºC)	$T_{cond,out}$ (ºC)	error margin
1	17	43	48.5	0.26
2	11	41	45.5	0.13
3	11	39	45.5	0.25

Figure 4.5: Training results of a cluster. The orange-shadowed region represents the error margin of the prediction.

4.4.2 Fault detection

In order to validate the fault detection part of the FDD system under test, a set of indicators will be used. These indicators are:

False alarm rate (false alarm rate (FAR)): it represents the fraction of erroneous fault warnings with respect to the sum of non-faulty and erroneous detection by the FDD system. In the equation below False Positive represents raising a warning for a non-existent fault.

$$FAR = \frac{\text{False Positive}}{\text{False Positive} + \text{True Negative}} \tag{4.1}$$

Missed detection rate (MDR): it represents the fraction of undetected faults with respect to the sum of detected and undetected faults by the FDD system. In the equation of MDR below, a False Negative implies that under the presence of a fault the algorithm does not raise any warnings.

$$MDR = \frac{\text{False Negative}}{\text{False Negative} + \text{True Positive}} \tag{4.2}$$

The Accuracy indicator represents the fraction of correct fault warnings with respect to the total fault warnings given by the FDD system.

$$Accuracy = \frac{\text{True positive}}{\text{True positive} + \text{False Positive}} \tag{4.3}$$

The Detection time (DT) is time since the COP residual (difference between real and predicted COP) is higher than 0.05 until the system raises a warning on COP drift.

$$DT = t_{COPWarning} - t_{faultStart} \qquad (4.4)$$

The Misdiagnosis rate (MR) indicator represents the capability of the FDD for correctly diagnose the faults detected. In the equation below False Diagnosis implies that a fault is detected but the diagnosis does not match the real fault.

$$MR = \frac{\text{False Diagnosis}}{\text{False Diagnosis} + \text{True Diagnosis}} \qquad (4.5)$$

The indicators presented above are related to the performance of the FFD model and its implementation. An ideal FFD system will achieve a FAR=0%; MDR=0%; Accuracy=100%; DT=10 min and MR=0. The DT of 10 minutes is the minimum for this algorithm, as it is the period needed to a consistent fault.

The $FIR_{COPdiagno}$ indicator represents the fault impact ratio (FIR) value for the COP, which is calculated as the ratio between the feature at fault and nominal fault free conditions for COP, when the system is able to diagnose a fault. A FIR_{COP}=1, means that there is no impact on the COP. It gives an indication of the degree of deterioration of the system when the FDD system is able to isolate a fault.

$$FIR_{COP} = 1 - \frac{COP_{unfaulted} - COP_{fault}}{COP_{unfaulted}} \qquad (4.6)$$

Figure 4.6 shows how the fault detection works. The COP from the heat pump is far from the prediction due a fault, LL in this case. With this difference, each data point increases the fault ratio. When the time period ends, if the fault ratio is above 80%, the warning flag is triggered.
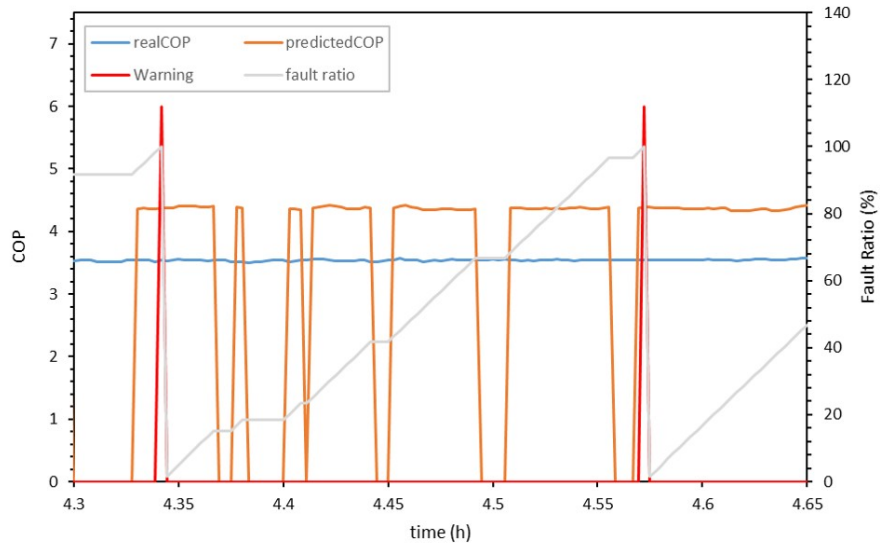
Figure 4.6: Fault detection for a LL fault in a static test. The fault ratio is the accumulated number of deviations in a certain time period. After this period, if the fault ratio is above 80%, a warning is triggered.

Table 4.2 shows the indicators for all the static tests. A one-hundred per cent of accuracy and 0 FAR indicates that this is a robust method. In this way, the user can be sure that no warning can be a false alarm.

Table 4.2: Performance values for the FDD. "-": FDD did not reach a prediction.

Code	FAR (%)	MDR (%)	Accuracy (%)	DT (min)	FIR_{COP}	COP drift (%)
EF10.1	0	-	100	-	1.00	0
EF10.2	0	-	100	-	1.00	0
EF10.3	0	-	100	-	0.99	1
EF10.4	0	-	100	-	0.99	1
EF10.5	0	-	100	-	0.98	2
EF10.6	0	33	100	22	0.97	3
EF10.7	0	16	100	9	0.96	4
EF10.8	0	19	100	5	0.95	5
EF12.1	0	-	100	-	0.99	1
EF12.2	0	-	100	-	0.99	1
EF12.3	0	-	100	-	0.98	2
EF12.4	0	-	100	-	0.97	3
EF12.5	0	-	100	-	0.97	3
EF12.6	0	-	100	-	0.96	4
EF12.7	0	-	100	-	0.94	6
EF12.8	0	16	100	11	0.93	7
CVL10.1	0	-	100	-	1.00	0
CVL10.2	0	-	100	-	1.00	0
CVL10.3	0	-	100	-	1.00	0
CVL10.4	0	-	100	-	0.98	2
CVL10.5	0	31	100	14	0.78	22
CVL10.6	0	15	100	6	0.71	29
CVL10.7	0	-	100	-	0.79	21
CVL12.1	0	-	100	-	1.00	0
CVL12.2	0	-	100	-	1.00	0
CVL12.3	0	-	100	-	1.00	0
CVL12.4	0	19	100	13	0.89	11
CVL12.5	0	0	100	6	0.69	31
CVL12.6	0	30	100	10	0.53	47
LL10.1	0	-	100	-	1.00	0
LL10.2	0	23	100	22	0.93	7
LL10.3	0	31	100	17	0.86	14
LL10.4	0	-	100	12	0.82	18
LL10.5	0	33	100	19	0.74	26
LL10.6	0	26	100	17	0.65	35
LL12.1	0	-	100	-	0.98	2
LL12.2	0	33	100	17	0.87	13
LL12.3	0	25	100	7	0.81	19
LL12.4	0	7	100	15	0.76	24
LL12.5	0	-	100	-	0.69	31
RO10	0	33	100	17	0.79	21
RO12	0	33	100	13	0.81	19

Figure 4.7 shows the FIR_{COP} versus the absolute FI of each fault. The LL fault is not represented as the FI could not be determined. Except for OC, for higher loads, the COP drift is higher. OC and CVL have a high impact on the COP.
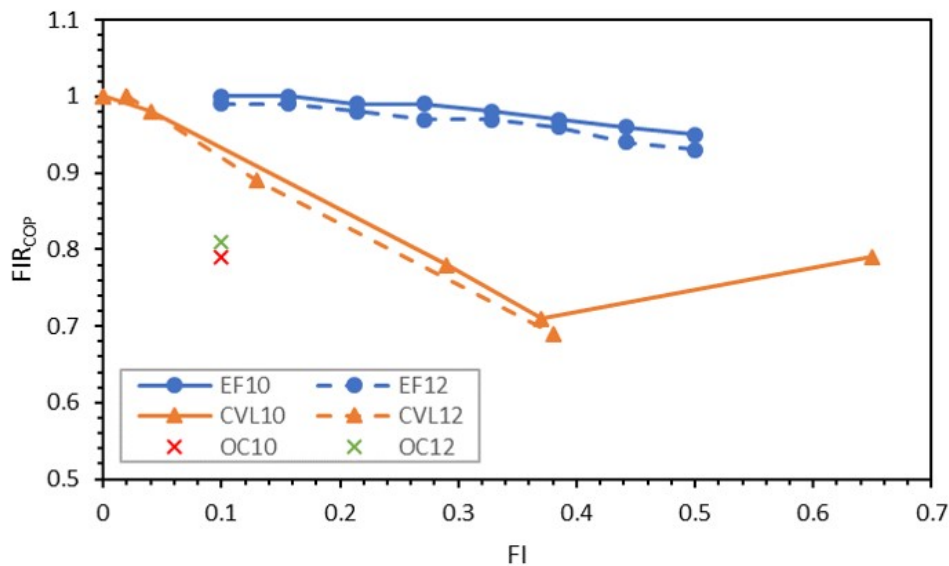

Figure 4.7: Absolute fault intensity versus COP fault impact ratio for each fault and load.

The MDR values are very dependent on the test itself. A false negative is considered when the algorithm detects 10 minutes of steady state data and the COP has decreased 0.05 and the FDD algorithm does not trigger a warning. As the tests have a duration of 60 minutes and discarding all the noisy data, there are low numbers of those periods. Therefore, the extension of the tests to 2 hours would improve this indicator. The DT is below 20 minutes. Without considering the unsteady area at the beginning of each test due to the FI increase, the DT is usually 10 minutes. The $FIR_{COPdiagno}$ is not shown directly as it can be misleading. This indicator gives a value of the COP drift when the fault is first diagnosed, but for faults like RO and LL, the FIR_{COP} increases fast with lower fault levels. Therefore, it may seem that the FDD cannot diagnose for lower FIR_{COP}, but it is because there is no more data with lower FIR_{COP}. In the same line, it can be stated that the algorithm detect COP drifts below 7% as it can be seen in the EF and LL faults. For the higher levels of CVL the algorithm could not predict because the condenser temperatures are out of the trained conditions, as the heat pump cannot cover the demand.

4.4.3 Fault diagnosis

The diagnosis methodology is based on trend values obtained from a literature review. As can be seen in Table 3.4 in section 3, the trends for this heat pump are different from the ones published in the literature. A test made with the old trend-chart showed that none of the test faults could be diagnosed correctly. E.g. for EF, the older version of the diagnosis module expected the T_{co} to increase, but it remains the same in the tests, therefore it will not be diagnosed as EF. Therefore, the diagnosis module was updated with the trends for this heat pump. The results of Misdiagnosis rate (MR) with this change is shown in Table 4.3. With the update, there is no misdiagnosis for any fault. However, for EF and higher demands of CVL, the algorithm could not diagnose the fault.

The differences between the trends obtained from literature and the ones obtained from the tests showed that this diagnosis method could not be generalized to other heat pump typologies. If more tests are made with differ-

ent variable-speed heat pumps, this method could be more flexible and less specific to the heat pump typology. However, the diagnosis module was not an objective of the TRI-HP project. Because of that, the diagnosis module could be improved as a result of future research projects.

Table 4.3: MR values for the updated diagnosis module

Code	MR (%)
EF10	-
EF12	-
CVL10	0
CVL12	0
LL10	0
LL12	0
RO10	0
RO12	0

5 CONCLUSIONS AND FUTURE STEPS

This deliverable describes the methodology and the experimental validation of the developed FDD algorithm. The FFD algortihm was first developed using data obtained emulating faults on a heat pump model implemented in Modellica and literature data. Afterwards it has been validated with real heat pump faults.

Different faults have been emulated on a variable speed compressor heat pump. Using the data from normal behaviour for training, the fault data has been used to test the FDD. Some parameters as the steady-state detector and the diagnosis chart have been adapted respect to the previous implementation using data obtained from a numerical heat pump model. However, the detection procedure has remained the same. The algorithm has detected all the faults before a high COP drift and diagnosed some of them. The main conclusions derived from this work are the following:

- The input variables for the regression model must pertain to the external conditions of the heat pump. In the beginning, the compressor speed was one of those input variables. However, in the majority of faults, the compressor speed changes with the same environmental conditions. Therefore, the algorithm will be in a situation not trained, and the prediction could be erroneous.
- The compressor speed is a crucial feature to diagnose faults. Although other indicators as refrigerant mass flow and electric power consumption can be related, the compressor speed is a feature that can indicate a possible fault.
- The fault emulation has contributed new data to the field. There are few studies about the fault impacts on variable-speed heat pumps. The data obtained in this work will be helpful for future developments.
- The FDD system has a performance that fulfils project's quantitative objectives of performance loss detection sensitivity. It can detect fault behaviour with a COP performance loss around 7 % with a 10 minutes response time, while the project goal was to detect a 10 % COP drift. The detection time threshold has increased compared to the theoretical results of the FDD using simulated data. However, this was expected, due to the noise and measurement uncertainty.
- The diagnosis module could diagnose correctly four of the five different faults. But it may not have the same results for different heat pump types. The expert knowledge methodology depends on the developer and the experience in the field. If more data become available about faults on different variable speed heat pumps, this method could be used in different heat pump technologies.

The detection algorithm was developed in Python and run from an industrial computer in the laboratory. However, to test the method portability, the same algorithm has been working real-time in a Raspberry Pi [1], which is a portable, low-cost computer. The results are the same shown in this document. In future, this FDD needs to be included and tested in a portable platform in the field.

Bibliography

[1] "What is a Raspberry Pi?" [Online]. Available: https://www.raspberrypi.org/help/what-is-a-raspberry-pi/

[2] S. Katipamula and M. R. Brambley, "Review article: Methods for fault detection, diagnostics, and prognostics for building systems—a review, part II," *HVAC and R Research*, vol. 11, no. 2, pp. 169–187, 2005.

[3] P. Domanski, H. Henderson, and W. Payne, "Sensitivity analysis of installation faults on heat pump performance. nist technical note 1848," Tech. Rep., 2014.

[4] T. Péan and J. Salom, "Laboratory facilities used to test energy flexibility in buildings," IEA EBC Annex 67 Energy Flexible Buildings, Tech. Rep., 2017. [Online]. Available: http://www.annex67.org/media/1373/lab-description-report-first-edition.pdf

[5] D. Noël, C. Teuillières, P. Rivière, O. Cauret, and D. Marchio, "Experimental Characterization of Fault Impacts on the Functioning Variables of an Inverter Driven Heat Pump," *10th International Conference on System Simulation in Buildings*, no. January 2019, 2018.

[6] M. Kim and M. S. Kim, "Performance investigation of a variable speed vapor compression system for fault detection and diagnosis," *International Journal of Refrigeration*, vol. 28, no. 4, pp. 481 – 488, 2005. [Online]. Available: http://www.sciencedirect.com/science/article/pii/S0140700704002579

[7] H. Cheung and J. E. Braun, "Modeling of fault impacts for a multi-split ductless heat pump system ," *IEA Heat Pump Conference 2014*, 2014.

[8] M. Kim, W. V. Payne, and P. A. Domanski, "Cooling mode fault detection and diagnosis method for a residential heat pump," *National Institute of Standards and Technology Special Publication 1087*, p. 98, 2008.